

Article

A New Radiative Model Derived from Solar Insolation, Albedo, and Bulk Atmospheric Emissivity: Application to Earth and Other Planets

Luke Swift

Geoscientist, 21 London Way, Perth 6150, Australia; lukeswift@swiftgeoscience.net

Received: 18 April 2018; Accepted: 27 May 2018; Published: 14 June 2018



Abstract: This study develops an equilibrium radiative model based on a quasi-adiabatic atmosphere that quantifies the average surface flux of a planetary body as a function of absorbed solar radiation P and the bulk emissivity of the atmosphere with respect to surface radiation ϵ . The surface flux is then given by $P/(1 - \epsilon)$, and I define the scaling term $1/(1 - \epsilon)$ as the greenhouse factor. The model is applied to all of the rocky planets in the solar system to determine their greenhouse factors, and accounts for the diversity of planetary surface fluxes. The model is modified to allow for a top of atmosphere non-equilibrium state, which when compared with a recent observation-based model of the Earth energy budget, predicts the Earth's radiative fluxes to within the uncertainty ranges of that model. The model developed in this study is able to quantify the changes in Earth's surface flux caused by changes in bond albedo and atmospheric bulk emissivity by using the surface temperature, ocean heat content, incoming solar radiation and outgoing longwave radiation records. The model indicates an increase in absorbed solar radiation over the time period from 1979–2015 of the order of 3 W/m^2 , which was caused by a decrease in planetary bond albedo. The time-series albedo generated by the model is in agreement with Clouds and Earth's Radiant Energy System (CERES) derived albedo over the period from 2000–2015. The model also indicates a slight decrease in atmospheric bulk emissivity over the same period. Since atmospheric bulk emissivity is a function of the sum of all of the greenhouse gas species, a simultaneous decrease in atmospheric water vapor may offset the effect of the well-documented increase in the non-condensing greenhouse gases over the period, and result in an overall net decrease in bulk emissivity. Atmospheric water vapor datasets partially support the conclusion, with the International Satellite Cloud Climatology Project (ISCCP) data supporting a decrease. The NASA Water Vapor Project (NVAP-M) data supports a decrease in atmospheric water content over the period 1998–2008, but not over the longer period of 1988–2008. The model indicates that the decrease in planetary albedo was the driver for the increased surface flux over the stated period.

Keywords: greenhouse effect; greenhouse factor; atmospheric energy budget; adiabatic radiative model; planetary surface temperature

1. Introduction

Over the past 30 years, observations of radiative fluxes associated with Earth's atmosphere from satellite and Earth-based platforms have improved our understanding of the Earth energy budget, as described by Rossow and Zhang (1995) [1], Kiehl and Trenberth (1997) [2], Wild et al. (2013) [3], Wild et al. (2015) [4] and Wild et al. (2017) [5]. These researchers have developed increasingly accurate empirical energy budgets based on direct observations and modeling results performed within global climate models. The results of Wild et al. (2015) represent the more recent results of Earth energy balance studies, in which direct observations from both surface and space, in combination

with 43 Coupled Model Intercomparison Project Phase 5 (CMIP5) models are used to determine the energy balance over land and oceans. Improvements in space-based observation systems enabled more accurate assessments of the top of atmosphere (TOA) radiation budgets, notably using the Clouds and Earth's Radiant Energy System (CERES). Wild et al. [3–5] used surface radiation observations from the global energy balance archive (GEBA), the Baseline Surface Radiation Network (BSRN), and ocean buoys to constrain surface fluxes, which cannot be directly measured from satellites. These authors recognize that the energy distribution within the climate system and at the Earth surface is less well-defined, with flux uncertainties that are larger than TOA fluxes. The global climate models that are used in determining and validating the surface fluxes consider all of the major natural and anthropogenic forcings, including change in atmospheric greenhouse gases, aerosol loadings, solar output, and land use.

Recent developments in the field of energy budget models include the sub-division of the energy budget into land and ocean components, which is the main subject of Wild et al. (2015) [4], building on their previous all-globe model in Wild et al. (2013) [3]. Future refinements and developments in the field will include large-scale surface albedo estimates and the representation of surface skin temperatures derived from upward surface flux. The better estimation of non-radiative flux components is also an area for further development. Another development is the further regionalization of energy budgets at a finer scale than global, land, and ocean means, which is currently underway in Europe.

This study aims to provide a new derivation of atmospheric radiative fluxes at the planetary scale, by determining the controls on average surface temperature as functions of incoming solar insolation, planetary bond albedo, and bulk atmospheric emissivity, which are applicable to Earth and other rocky planets in the solar system. I investigate the agreement between this model and the global energy budget of Wild et al. (2015) [4] and the output of global climate models. A further aim of this study is to calculate the time-series behavior of Earth's radiative fluxes, absorbed solar insolation, and emissivity to identify possible causes of the increased surface flux over the period 1979–2015. The derivation of the more uncertain surface fluxes [3] is of particular interest to this study.

Importantly, the model derived in this study is impartial, in the sense that no restrictions are placed *ab initio* on the behavior of the independent variables of solar insolation, albedo, and bulk atmospheric emissivity, which together determine the upward surface flux and top of atmosphere fluxes in the equilibrium model. The behavior of these variables is determined from the time-series datasets of incoming solar insolation, planetary bond albedo, and bulk atmospheric emissivity. The non-equilibrium model is thus capable of identifying, and in fact does identify, a decrease in the bulk atmospheric emissivity over the period 1979–2015. This is possible because changes in atmospheric water vapor, as well as the increase in atmospheric non-condensing greenhouse gases, contribute to the bulk emissivity. Decreasing atmospheric water vapor may offset the effect of increases in the other greenhouse gas species, and reduce atmospheric bulk emissivity. Atmospheric models that assume that increasing non-condensing greenhouse gas abundance must result in an increased bulk emissivity cannot identify a scenario of decreasing bulk atmospheric emissivity by definition.

Section 2 lists the datasets used in the validation of the adiabatic radiative model. Section 3 summarizes the model, then derives the equilibrium and non-equilibrium radiative models for an idealized planetary atmosphere. The radiative model uses the properties of a one-dimensional quasi-adiabatic atmosphere, in which the atmosphere acts as a non-symmetric emitter of absorbed radiation. The model is then validated by comparison with the land plus sea model of Wild et al. (2015) [4] in Section 3.3, and is shown to be in agreement.

The equilibrium model is applied to other planetary bodies in the solar system in Section 3.4, and their greenhouse factors are discussed. The application of the non-equilibrium model to Earth over the period 1979–2015 is discussed in Section 3.5. Outcomes of the model that at first glance appear counterintuitive—in particular a decrease in the strength of the greenhouse factor over the period—are explained with reference to the definition of the atmospheric bulk emissivity.

In Section 4, further features of the model are discussed, and comparisons are made with the means of CMIP5 models. A more detailed description of how the model quantifies the components of downwelling longwave radiation (DWLR) is given, and shows how increased absorbed solar radiation profoundly affects DWLR.

2. Materials and Methods

The adiabatic radiative model is derived from application of the Stefan-Boltzmann law to an atmosphere that is modeled with a non-emitting top surface, as described in Sections 3.1 and 3.2. Analysis of the model uses satellite-based measurements of outgoing longwave radiation and incident total solar insolation, the surface temperature record, and the ocean heat content record. The outgoing longwave radiation dataset is the High-resolution Infrared Radiation Sounder (HIRS) v2.2. OLR provided by the National Center for Environmental Information [6], with monthly values averaged over the globe. The solar insolation dataset is from the Physikalisch-Meteorologisches Observatorium Davos and World Radiation Centre (PMOD/WRC) [7]. For surface temperatures, absolute values are required for the direct calculation of a proxy for surface radiative flux. Global averaged monthly values of NOAA Extended Reconstructed Sea Surface Temperature (ERSST) v5 [8] over oceans and Global Historical Climatology Network and Climate Anomaly Monitoring System (GHCN CAMS) [9] over land were weighted 70.8% and 29.2%, respectively, to derive average surface temperatures. These datasets are obtained via the Koninklijk Nederlands Meteorologisch Instituut (KNMI) Climate Explorer website [10]. Other evidence for the implications of the adiabatic model includes the atmospheric Total Water Vapor measurements from the D2 dataset provided by the International Satellite Cloud Climatology Project (ISCCP) [11], using mean monthly values averaged over the globe, and average annual Total Precipitable Water from the NASA Water Vapor Project (NVAP-M) dataset [12] provided by Vonder Haar et al. (2012) [13]. Ocean heat content data for use in the non-equilibrium radiative model was obtained from Cheng et al. (2017) [14]. Planetary parameters for solar insolation and surface temperature are taken from the NASA planetary data sheets. Titan data was taken from Yelle et al. (1997) [15]. CERES [16] top of atmosphere shortwave flux—all sky data and incoming solar flux data—were used to validate albedo derived from the radiative model over the period 2000–2015.

3. Results

3.1. Statement of the Model

Consider a radiatively-balanced one-dimensional atmosphere—planet system that absorbs an amount of incident solar insolation P in W/m^2 . Then, the upward radiative flux emitted by the planetary surface is equal to $P/(1 - \epsilon)$ W/m^2 , where ϵ , $0 \leq \epsilon < 1$ is the dimensionless value of bulk emissivity of the atmosphere with respect to the emitted surface radiation. I define the scaling term $1/(1 - \epsilon)$ as the greenhouse factor, because it quantifies the greenhouse effect as a multiplier of the absorbed solar radiation. See Figure 1.

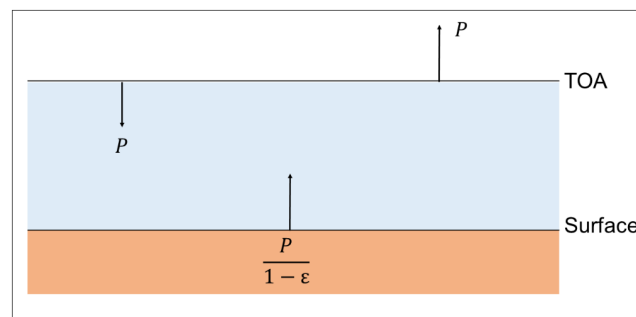


Figure 1. Surface amplification of absorbed solar insolation P . ϵ , $0 \leq \epsilon < 1$ is the bulk emissivity of the atmosphere with respect to the surface radiation. Units W/m^2 . TOA = top of atmosphere.

3.2. Derivations of the Equilibrium and Non-Equilibrium Radiative Models

3.2.1. Properties of an Adiabatic Atmosphere

The adiabatic barometric Equations (1)–(3) describe the pressure $p(z)$, density $\rho(z)$, and temperature $T(z)$ profiles at height z , as a power function of their surface or other nominal values (p_o, ρ_o, T_o, z_o), gravity g , and the specific heats of the atmosphere by constant pressure C_p and constant volume C_v [17].

$$p(z) = p_o \left(1 - \frac{g}{C_p T_o} (z - z_o) \right)^{C_p / (C_p - C_v)} \quad (1)$$

$$\rho(z) = \rho_o \left(1 - \frac{g}{C_p T_o} (z - z_o) \right)^{C_v / (C_p - C_v)}, \quad (2)$$

$$T(z) = T_o - \frac{g}{C_p} (z - z_o) \quad (3)$$

Within such an atmosphere, gaseous molecules are free to ascend by exchanging kinetic energy with gravitational potential energy. As such, the atmosphere has a well-defined upper boundary at height $(z - z_o) = C_p T_o / g$, at which point all of the molecular kinetic energy is converted to gravitational potential energy, and the theoretical temperature, pressure, and molecular density is zero. A non-zero top of atmosphere temperature is unstable in an adiabatic model. Let us consider that some fraction nP , $0 < n < 1$ of solar insolation P absorbed within the atmosphere is redirected upward and emitted up from the top surface. Then, considering the atmosphere as a radiative grey body, the top of atmosphere will have an effective temperature T_2 defined by $\sigma T_2^4 = nP$. Let the height of the top of atmosphere be z_2 . The atmospheric molecules at the top surface then have positive kinetic energy, and are free to rise to a new top of atmosphere at height $z_{top} = z_2 + C_p T_2 / g$, where, from Equation (3), all of the kinetic energy is once again converted to gravitational potential energy, and the temperature of the top of atmosphere is zero Kelvin and $n = 0$.

In the case of real atmospheres, including Earth, the absorption of solar insolation in the atmosphere disrupts an adiabatic temperature profile. However, application of the Stefan-Boltzmann law applies only to radiating surfaces, and so long as the boundary conditions are maintained, I am not concerned with internal deviations of temperature from the idealized adiabatic profile within the radiating body. In this sense, the model is quasi-adiabatic. These properties overcome the problem of a diffuse and poorly defined upper atmospheric boundary, and allow the atmosphere to be modeled as a radiative grey body with distinct upper and lower surfaces, to which the Stefan-Boltzmann law may be applied. When modeled in this way, the top of atmosphere is a non-radiating surface, since its theoretical adiabatic temperature is zero Kelvin, and the atmosphere is a fully anisotropic emitter, such that any atmosphere-absorbed radiation is re-emitted only through the bottom surface. This condition is crucial to the model.

3.2.2. Derivation of the Equilibrium Adiabatic Radiative Model

The atmosphere in Figure 2 is modeled as a grey body that is partially transparent to electromagnetic radiation. Applying boundary conditions of an adiabatic barometric temperature profile, the temperature at the top of the atmosphere is $T_2 = 0$ K. The bottom of the atmosphere has temperature T_1 . The planetary surface temperature is T_o . The base of the atmosphere is in contact with the surface, but is shown separately from the surface for the purpose of clarity in the figure.

The atmosphere–planet system receives total solar insolation S at the top of atmosphere (TOA). Geometrically averaged over a sphere, the amount $(1 - a)S/4$ enters the system, and an amount $aS/4$ is reflected, where a , $0 \leq a \leq 1$, is the dimensionless bond albedo, which comprises all of the solar insolation reflected from the atmosphere and the surface. Of the solar insolation entering the system, an amount $\mu(1 - a)S/4$ is absorbed by the atmosphere, and the remainder $(1 - \mu)(1 - a)S/4$ is transmitted through the atmosphere and absorbed by the planet surface. The dimensionless quantity

μ , $0 \leq \mu < 1$ is the bulk shortwave emissivity of the atmosphere with respect to solar radiation. Since the top of atmosphere is a non-radiating surface, the absorbed quantity $\mu(1 - a)S/4$ can only be re-radiated downwards to maintain radiative balance.

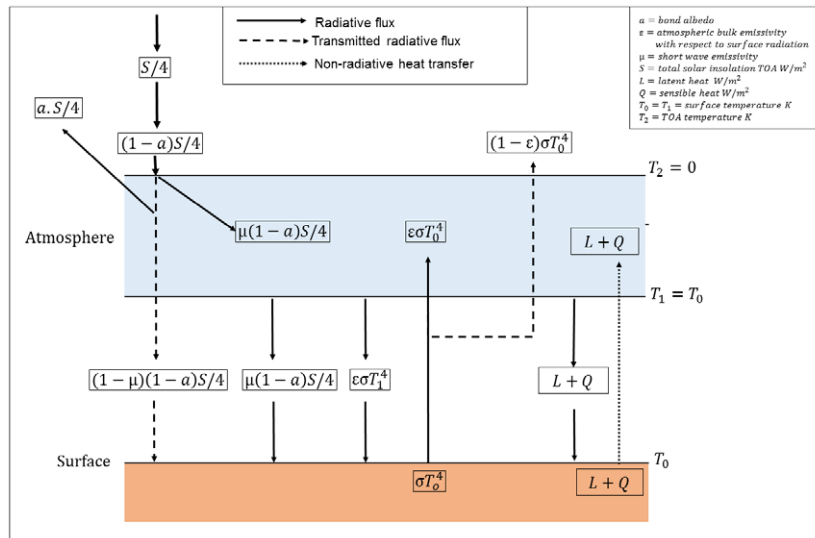


Figure 2. Equilibrium adiabatic radiative model. All of the units are in W/m^2 except temperatures T_0 , T_1 , T_2 , which are in Kelvin.

At the planet surface, the upward flux is σT_0^4 , where σ is the Stefan-Boltzmann constant. Of this radiative flux, an amount $\epsilon\sigma T_0^4$ is absorbed by the atmosphere, and $(1 - \epsilon)\sigma T_0^4$ is transmitted through the atmosphere and escapes the system, where ϵ , $0 \leq \epsilon < 1$ is the dimensionless bulk emissivity of the atmosphere with respect to the surface radiation. The absorbed component $\epsilon\sigma T_0^4$ is re-emitted downward to the surface. The transmitted portion $(1 - \epsilon)\sigma T_0^4$ comprises the entirety of the outgoing longwave radiation (OLR) of the system. Thus, to maintain the radiative balance of the entire system, it follows that at radiative equilibrium:

$$(1 - a)S/4 = (1 - \epsilon)\sigma T_0^4 \tag{4}$$

The radiative model allows for non-radiative energy transfer from the surface to the atmosphere, in the form of the latent heat of vaporization of water per unit time L , and sensible heat transfer per unit time Q through conduction. This energy must be re-emitted as longwave radiation down from the atmosphere; hence, these transfers result in an increase in total downwelling longwave radiation. I assume that the equivalent value of downwelling radiation is re-consumed by the same processes so that downwelling radiation ($L + Q$) does not on average contribute to a surface temperature increase. From considerations of radiative and energy transfer balance in Figure 2, it follows that:

$$T_1 = T_0. \tag{5}$$

This condition also prevents a discontinuity in temperature at the planet–atmosphere boundary. Alternatively, I consider that since the base of atmosphere is in contact with the surface, then in an equilibrium state, these must have the same temperature on average over the planet. It then follows from the radiative balance that:

$$T_1 = T_0 \Leftrightarrow T_2 = 0. \tag{6}$$

The physical interpretation of $T_2 = 0$ is that the TOA can be regarded as a non-radiating surface in the grey body model. Note that this condition is theoretically supported from both the convective (adiabatic) modeling from Equations (1)–(3), and radiative modeling from Equations (5) and (6).

From Equation (4), the term σT_0^4 is now redundant in the model, and can be replaced to yield the radiative model as shown in Figure 3. Radiative fluxes are thereby expressed as functions of S , a , ϵ , μ , L & Q . Note that the upward surface flux and top of atmosphere fluxes are expressed in terms of the three independent variables S , a , and ϵ . The remaining variables L , Q , and μ do not affect the upward surface flux or TOA fluxes. By replacing for absorbed solar insolation $P = (1 - a)S/4$ in Figure 3, and ignoring all of other fluxes except at top of atmosphere and upward radiative surface flux, I reproduce Figure 1, which is the statement of the model in Section 3.1. It is important to note that the quantity P is not an independent variable; it is used as a convenient simplification of the algebraic expressions for flux components in Figures 1, 3 and 4. P is entirely dependent on the two independent variables S and a . If I consider S as a constant, which is approximately correct, then changes in albedo a determine changes in P , and not vice versa.

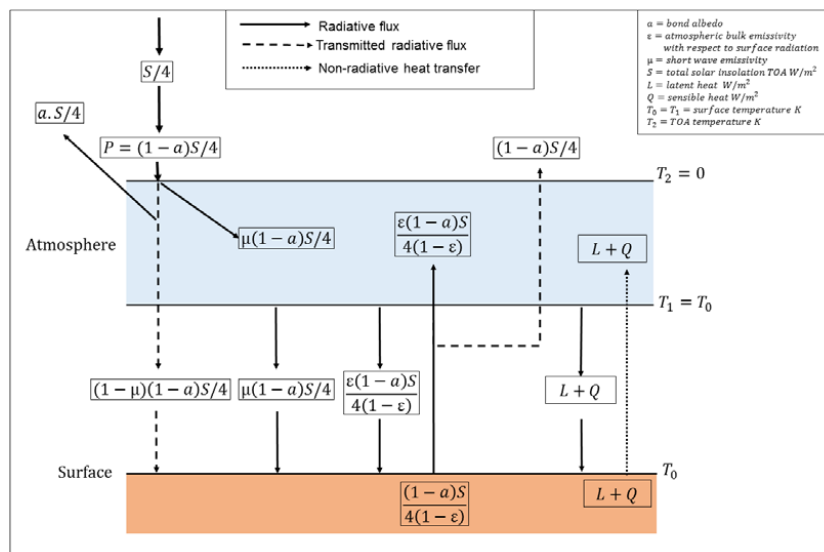


Figure 3. Equilibrium adiabatic radiative model with fluxes given as functions of S , a , ϵ , μ , L & Q . All of the units are in W/m^2 except temperatures T_0 , T_1 , T_2 , which are in Kelvin.

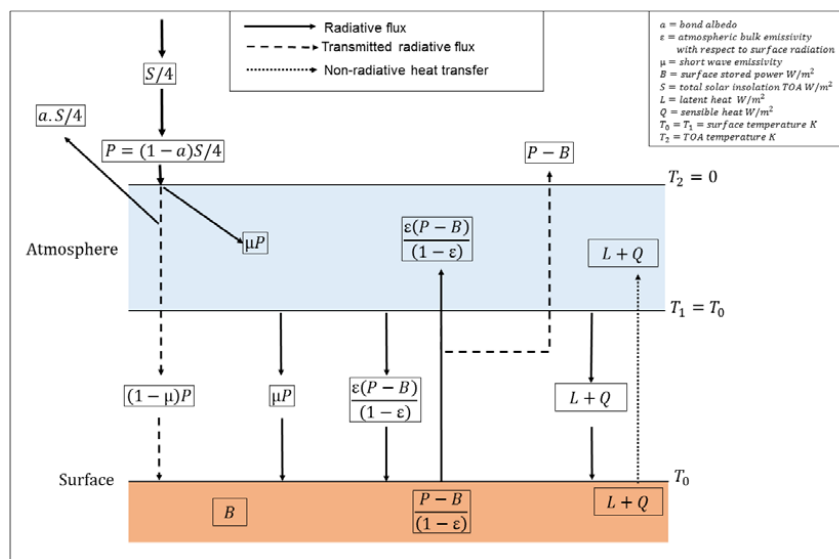


Figure 4. Non-equilibrium adiabatic radiative model with fluxes given as functions of P , ϵ , μ , B , L & Q . All of the units are in W/m^2 , except temperatures T_0 , T_1 , T_2 , which are in Kelvin.

3.2.3. Derivation of the Non-Equilibrium Adiabatic Radiative Model

A refinement of the equilibrium model shown in Figure 4 allows for transitional, non-equilibrium radiative states associated with thermal ramp-up or ramp-down of the surface following changes in the total downwelling radiation. A change in downwelling radiation at the surface can arise from a change in P or bulk atmospheric emissivity ε . Such a perturbation results in an imbalance between the surface absorbed and surface emitted flux, and also results in an imbalance between the absorbed and emitted flux at the top of atmosphere. In the case of an increase in downwelling radiation, the surface temperature must increase to regain radiative equilibrium with the downwelling radiation. Some fraction B of the increase in downwelling radiation is absorbed and retained in the surface, and results in a monotonic increase of the surface temperature. B in W/m^2 is the rate of energy accumulation and storage of energy E (J/m^2) in the surface, such that $B = dE/dt$. In the case of Earth, the thermal ramp-up largely comprises the absorption of downwelling radiation in the oceans (Hansen et al., 2005) [18], and observations of ocean heat content E are used to quantify B .

The flux equivalent of B is unavailable for surface emission, and I adjust the flux components appropriately as shown in Figure 4. Consider conservation of energy at the surface:

$$P + \varepsilon\sigma T_0^4 + L + Q = \sigma T_0^4 + L + Q + B \quad (7)$$

$$\text{thus } \sigma T_0^4 = (P - B)/(1 - \varepsilon) \quad (8)$$

The surface flux is then given by $(P - B)/(1 - \varepsilon)$, and outgoing longwave radiation is $(P - B)$. As we shall see below, this non-equilibrium state describes the condition of the Earth, as shown in the radiative model of Wild et al. (2015).

In the case of a decrease in the downwelling radiation, the surface temperature must decrease in order to regain radiative equilibrium; this equates to B having a negative value, and energy emitted by radiation from the surface temporarily exceeds energy absorbed, and the surface temperature therefore decreases. Let the amount of energy required to be lost or gained by the surface to regain radiative equilibrium with downwelling radiation be J (in joules per meter squared), then:

$$J = \int_{t_0}^{t_{equ}} B(t).dt, \quad (9)$$

where t_0 is the time of the initiation of the perturbation, and t_{equ} is the time at which equilibrium is regained. When $B = 0$, the model reverts to the equilibrium state of Figure 3.

3.3. Validation of the Model by Comparison with Observations

Table 1 lists the values for atmospheric radiative and non-radiative flux components as compiled by Wild et al. (2015), (see also Figure 5), and the calculated equivalents in the adiabatic radiative model using the parameters shown in the “Value” column. The observation-based model, with a top of atmosphere radiative imbalance, is equivalent to the non-equilibrium adiabatic radiative model of Figure 4. The values for variables a , μ & ε are calculated directly from the Wild et al. model using their “Best Estimate” values:

$$a = (\text{reflected solar}/\text{total TOA solar}) = 100/340 \quad (10)$$

$$\mu = (\text{atmosphere absorbed solar}/\text{absorbed solar}) = 80/240 \quad (11)$$

$$\varepsilon = 1 - (\text{outgoing radiation}/\text{emitted surface radiation}) = 1 - 239/398 \quad (12)$$

These observation-based values are then used to calculate each radiative flux in the model using the parameters shown in Figure 4. The adiabatic model uses the value of $0.6 \text{ W}/\text{m}^2$ for “Imbalance”, as determined by Wild et al. for the value of B . Refer to Wild et al. (2015) for the derivation of their

uncertainty ranges, as shown in Table 1, which are derived from $\pm 2 \text{ W/m}^2$ accuracy levels in CERES data and 2σ uncertainties in ground-based flux measurements from GEBA and BSRN.

The values for $(L + Q)$ in the adiabatic radiative model are also taken directly from the estimates of Wild et al. (2015). These values are only relevant to determining the total downwelling atmospheric radiation, but, as discussed above, do not contribute to the globally averaged surface radiative flux. The adiabatic model uses only a bulk value for albedo, hence, the Wild et al. model value for “Solar reflected surface” is already incorporated into a of the adiabatic model, and the value “Solar down surface” is not required.

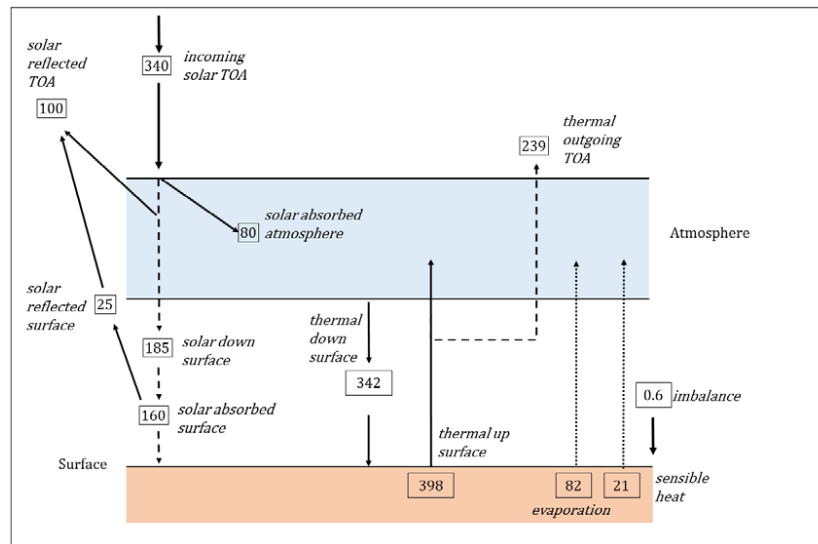


Figure 5. Observation-based land and sea energy budget diagram, modified after Wild et al. (2015) [4]. All of the units are in W/m^2 .

Table 1. Comparison of fluxes reported by Wild et al. [4] and calculated using the adiabatic radiative model. Values for the variables are derived directly from Wild et al. using the “Best Estimate” values, and calculated in the adiabatic model using the formulae in the Value column.

Unit	Wild et al. Model		Adiabatic Radiative Model	
	Best Estimate	Uncertainty Range	Value	Calculated
Variables				
$S \text{ W/m}^2$	1360		1360	
μ	0.3333		0.3333	
ϵ	0.3995		0.3995	
a	0.2941		0.2941	
$P = (1 - a)S/4 \text{ W/m}^2$	240		$(1 - a)S/4$	240
Fluxes, W/m^2				
Incoming solar TOA	340	340–341	$S/4$	340
Solar absorbed by atmosphere	80	74–91	μP	80
Solar reflected TOA	100	96–100	$a.S/4$	100
Solar down surface	185	179–189	not used	
Solar absorbed surface	160	154–166	$(1 - \mu)P$	160
Solar reflected surface	25	22–26	not used	
Evaporation	82	70–85	-	-
Sensible heat	21	15–25	-	-
Evaporation + sensible heat	103	85–110	103^1	-
Thermal up surface	398	394–400	$(P - B)/(1 - \epsilon)$	398.6
Thermal outgoing TOA	239	236–242	$P - B$	239.4
Thermal down surface	342	338–348	$\epsilon(P - B)/(1 - \epsilon) + \mu P + L + Q$	342.3
Imbalance	0.6	0.2–1	$B = 0.6^1$	

¹ The value for “Evaporation + sensible heat” equates to $(L + Q)$ in the adiabatic model; “Imbalance” equates to B . These values in the adiabatic model validation are taken directly from Wild et al. [4].

The adiabatic model approximates the observed radiative fluxes to within the uncertainty ranges shown in Table 1, and closely approximates the “Best Estimate” values of Wild et al. It is noteworthy that the relatively simple adiabatic radiative model is able to closely approximate downwelling longwave radiation purely by considering absorbed solar insolation, rate of ocean heat storage, and the bulk atmospheric emissivity. This value is close to the best estimate for global mean downward thermal radiation derived by Wild et al. (2013) [3] (p. 3127) from 21 CMIP5/IPCC AR5 models.

3.4. Application of the Equilibrium Adiabatic Radiative Model to Planetary Bodies

The equilibrium adiabatic radiative model is applied to the four rocky planets [19] and one satellite, Titan, with the resulting calculated values for P , ϵ and greenhouse factor in Table 2. The positions of Mercury, Mars, Earth, Venus, and Titan are plotted on a graph of ϵ against $1/(1 - \epsilon)$ in Figure 6. This graph shows the relationship between bulk atmospheric emissivity and the greenhouse factor. (Note that this is a purely descriptive graph with no error estimation, since the greenhouse factor is derived directly from the atmospheric bulk emissivity, hence all of the planetary bodies in Table 2 will fall exactly on the curve). The greenhouse factor is dependent on the absolute mass of atmospheric greenhouse gases present, hence Venus, with the densest atmosphere dominated by greenhouse gases, has the greatest greenhouse factor of 112 units. Mars, with the most tenuous atmosphere, has a very small greenhouse factor. Mercury with no atmosphere has $\epsilon = 0$, and a greenhouse factor of 1, which is the trivial case application of the adiabatic model to planets without an atmosphere. Note that the greenhouse factor $1/(1 - \epsilon)$ is unbounded, and approaches infinity as ϵ approaches unity. Any sufficiently massive irradiated atmosphere can therefore in theory generate any high surface temperature, the closest example of which is the atmosphere of Venus; further research is required to apply the radiative model to the gas giants, which potentially have much higher greenhouse factors.

The equilibrium radiative model of Venus most clearly demonstrates the anisotropic nature of atmospheric emission. Of the $16,728 \text{ W/m}^2$ of surface flux, only 149 W/m^2 escapes the system as transmitted longwave radiation, and the remaining atmosphere-absorbed $16,579 \text{ W/m}^2$ is redirected into the surface, which is required to maintain the high surface temperature.

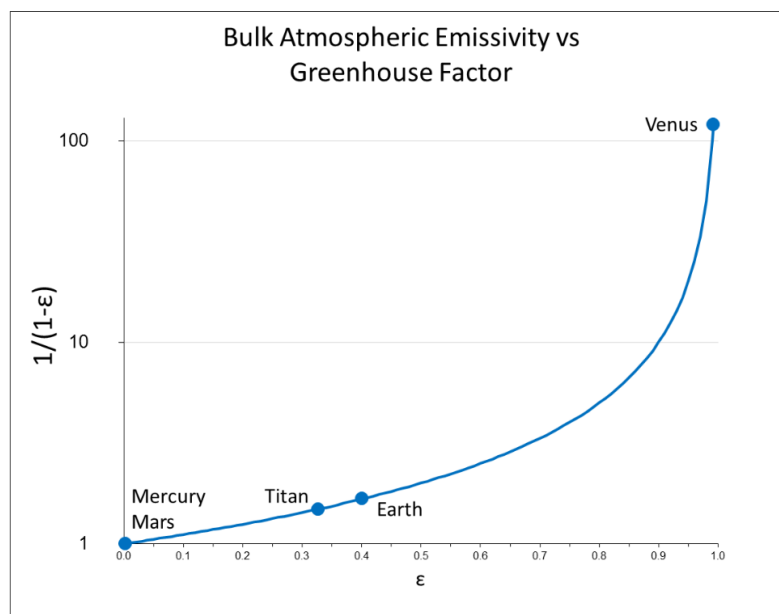


Figure 6. Positions of rocky planets and Titan on the bulk atmospheric emissivity versus greenhouse factor curve.

Table 2. Calculated greenhouse factors for rocky planets and Titan.

PARAMETER	Mercury	Venus	Earth ¹	Mars	Titan
Average surface temperature K	440	737	290	210	93
Total solar flux S W/m ²	9083	2601	1361	586	14.82
Absorbed solar radiation P W/m ²	2125	149	237	109.9	2.89
Albedo	0.07	0.77	0.3	0.250	0.22
Atmospheric bulk emissivity ϵ	0	0.991	0.407	0.0038	0.327
Average surface flux W/m ²	2125	16,728	400	110.3	4.30
Greenhouse factor	1	112	1.69	1.004	1.49

¹ Earth values 1982–1983 average, this study.

3.5. Application of the Non-Equilibrium Adiabatic Radiative Model to Earth

In the non-equilibrium radiative model, the Earth's surface flux is determined by solar insolation, albedo, bulk atmospheric emissivity with respect to the surface flux, and the rate of energy storage B into (or out of) the oceans. These quantities can be determined using time-series datasets of incoming top of atmosphere solar isolation S , outgoing longwave radiation (OLR), the surface temperature record T_0 as a proxy for surface flux, and ocean heat content as a proxy for stored energy. In this application, we must consider the adiabatic radiative model as nothing more than a template or framework by which we can evaluate the climate data sets. The model itself is impartial to the outcomes, that is, the model does not predict or constrain a priori how each of the independent variables S , B , ϵ , or a will change. The radiative model quantifies these variables using the following relationships:

$$|P| = |\text{OLR}| + B, \quad (13)$$

$$a = 1 - 4.(|\text{OLR}| + B)/|S|, \quad (14)$$

$$\text{bulk emissivity } \epsilon = 1 - |\text{OLR}|/\sigma T_0^4, \quad (15)$$

$$\text{greenhouse factor} = 1/(1 - \epsilon) = \sigma T_0^4/|\text{OLR}|, \quad (16)$$

$$\text{surface flux} = \sigma T_0^4. \quad (17)$$

The accuracy of HIRS 2.2 OLR [20] is estimated at ± 2 W/m² with respect to CERES, and the HadCRUT4 [21] total uncertainty estimates of the 95% confidence interval of all of the uncertainties described in the HadCRUT4 error model are applied to the combined ERSST v5 and GHCN CAMS temperature used for the proxy surface flux derivation in the graphs, as shown in Figure 7. B is approximated from dE/dt using the ocean heat content data. The rate of change in ocean heat over the period from January 1979 to June 1984 was estimated as $B = -0.27 \pm 0.12$ W/m² averaged over the globe, and over the period June 1984 to June 2015, it was estimated as $B = 0.67 \pm 0.12$ W/m². The uncertainty value is approximated from the maximum and minimum slopes over the second period allowed by the uncertainties in ocean heat content E from the data source in June 1984 and June 2015.

Figure 7 displays time-series graphs over the period 1979–2015 of absorbed solar insolation (Figure 7a), the greenhouse factor (Figure 7c), bond albedo (Figure 7d), surface flux (Figure 7e), and bulk atmospheric emissivity (Figure 7f), as generated by the radiative model. The ocean heat content from Cheng et al. (2017) is shown in Figure 7b.

Figure 7a shows that the model identifies an increase in the absorbed solar radiation in the order of 3 W/m² over the period. This increase is a direct result of the decrease in the bond albedo shown in Figure 7d, which shows a gradual decrease from a value of around 0.3 to 0.29 over the period 1979 to 1999, and then remains flat, with short-term fluctuations, over the period from 1999 to 2015. To validate the model-derived albedo, I added the CERES-derived albedo to the graph over the period 2000–2015 in Figure 7d, which is shown as the red line. In absolute terms, the values and the trends are

in reasonable agreement, giving some confidence in the model-generated values in the prior period of 1979–2000. This should not be surprising, as Equation (14) is derived from the definition of bond albedo, using the HIRS 2.2 OLR dataset and B to derive absorbed solar, and PMOD for incoming TOA solar. In Figure 8, albedo is expressed as top of atmosphere anomalies in W/m^2 . The blue curve is generated from the adiabatic model using HIRS 2.2, as well as incoming solar and ocean heat content data; the red curve shows earthshine values as reported by Palle et al. (2016) [22], and the black curve is CERES data obtained in May 2018. Over the common overlap period between 2000–2014, the trends are $-0.038 W/m^2$, $0.020 W/m^2$, and $-0.022 W/m^2$ per annum for the adiabatic model, earthshine, and CERES anomalies respectively; that is, trends are near flat and in general agreement. The adiabatic model shows some minor deviation from the other datasets over the period 2008–2011, of an order of less than $1 W/m^2$.

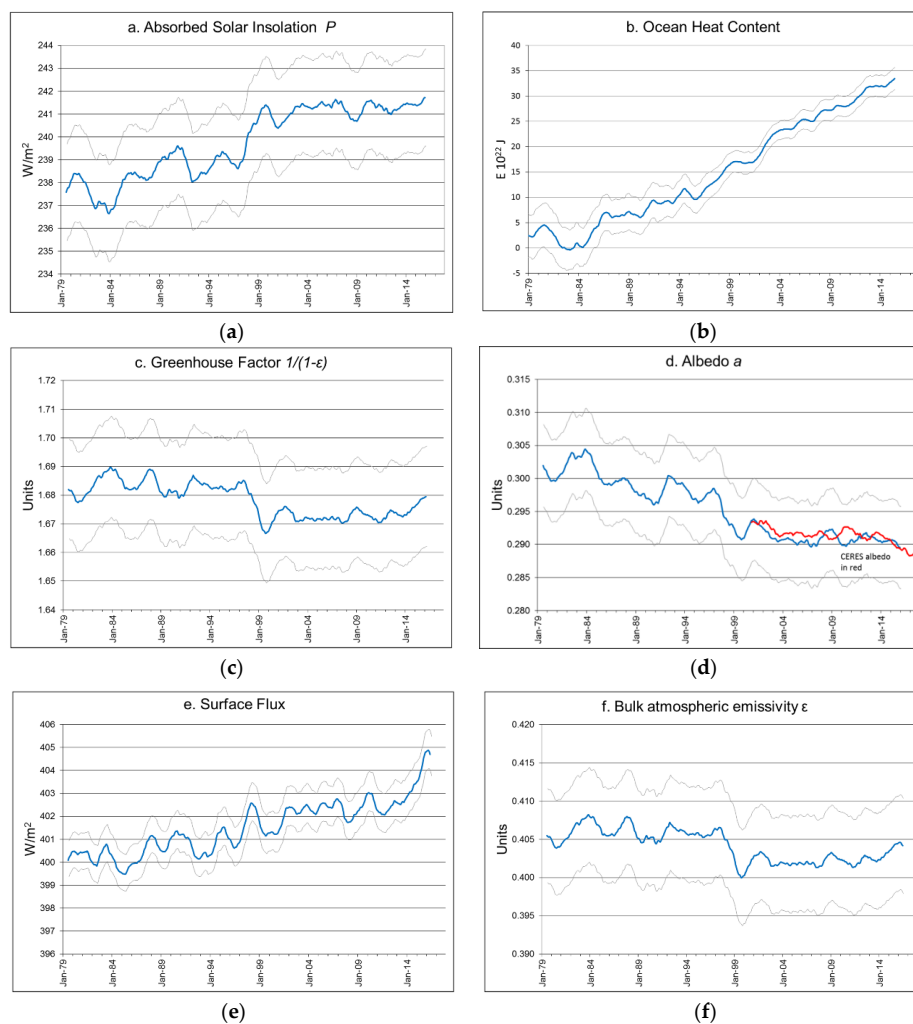


Figure 7. Center-averaged 12 monthly values for the period 1979–2015 for (a) absorbed solar insolation P ; (b) ocean heat content relative to 1958–1962 base period; (c) greenhouse factor; (d) bond albedo, with Clouds and Earth’s Radiant Energy System (CERES)-derived albedo in red; (e) surface flux; and (f) bulk atmospheric emissivity. Grey lines in (a,c,d,f) derived from the $2 W/m^2$ accuracy estimate of the HIRS 2.2. Absorbed solar insolation and surface flux graphs both show $10 W/m^2$ range over their y -axes.

Figure 7c shows the time-series behavior of the greenhouse factor. The model identifies a slight decrease in this value over the period, which is also reflected in Figure 7f, of atmospheric bulk emissivity. A decreasing greenhouse factor means a weakening of the greenhouse effect. An immediate objection to this model outcome is that the increasing atmospheric greenhouse gas concentrations

are well-documented over the time period. This objection is overcome when I consider that the bulk atmospheric emissivity ϵ is the sum effect of all of the greenhouse gases in the atmosphere. An increase in atmospheric non-condensing greenhouse gas concentration may be offset by a decrease in atmospheric water vapor, which is the dominant greenhouse gas; however, this model is not able to determine the magnitudes of the contributions of differing greenhouse gas species. There is differing evidence for decreasing atmospheric water content during the time period. Figure 9 shows graphs of Total Precipitable Water from the NVAP-M dataset [12] and Total Water Vapor from the ISCCP D2 dataset [11] over the period from 1988–2008. The ISCCP data support the interpretation of decreasing atmospheric water, particularly after 1998. The NVAP-M data show a decrease in atmospheric water over the period from 1998 to 2008, but of a much lower magnitude than the ISCCP data, and the overall trend from 1988 does not show a decrease. Hence, the NVAP-M data over the period from 1988–1998 do not support an interpretation of decreasing atmospheric water vapor.

Since the surface flux shown in Figure 7e is the product of the greenhouse factor and absorbed solar insolation minus B , that is $(P - B)/(1 - \epsilon)$, it is clear from the model that increasing absorbed solar radiation, caused by a lowering of the bond albedo, was the driver of increased surface temperature during the period 1979–2015, and also of the increase in ocean heat content, as shown in Figure 7b. The model does not identify a cause for the decrease in albedo; the model is impartial. I may speculate that a decrease in atmospheric water content, apart from lowering atmospheric bulk emissivity, also leads to a decrease in cloud cover and therefore to a decrease in albedo.

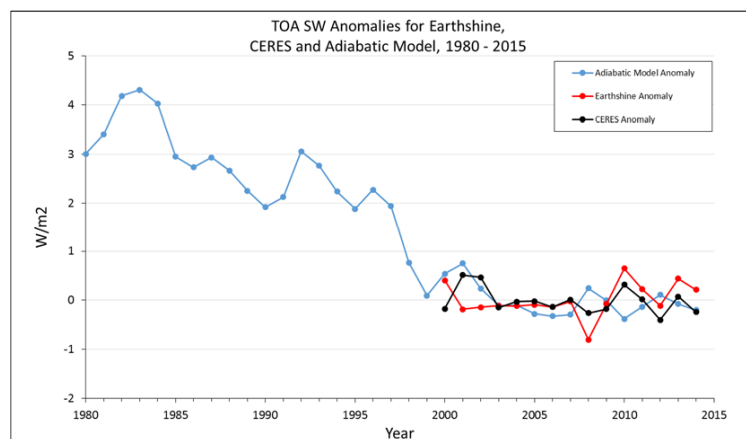


Figure 8. Top of atmosphere shortwave radiation anomalies, expressed in W/m^2 , for the adiabatic model (compared to 2000–2014 average), CERES (compared to 2000–2016 average), and earthshine (compared to 1998–2014 average) [22] datasets.

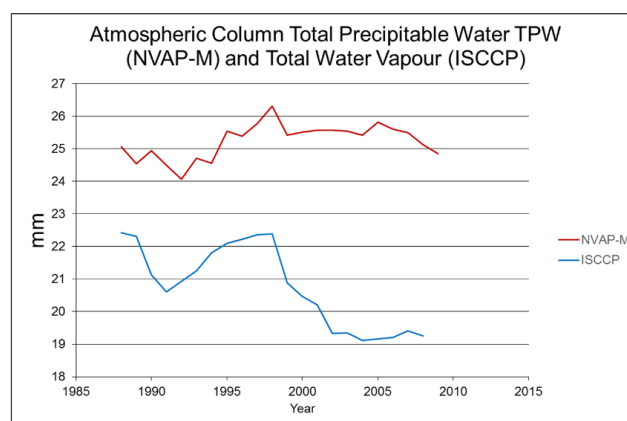


Figure 9. Estimates of global annual average atmospheric total precipitable water and total water vapor.

4. Discussion

The adiabatic radiative model, which was derived from a consideration of a theoretical non-radiating top of atmosphere, approximates average planetary surface flux as a function of absorbed solar radiation and a scaling factor, the greenhouse factor, which quantifies the greenhouse effect of an atmosphere on the surface temperature. The model is applicable to all of the rocky planets in the solar system. By allowing for the small non-equilibrium conditions on Earth quantified by changes in ocean heat content, the model was compared directly with the empirical, observation-based energy budget derived by Wild et al. (2015) [4], and was found to be in close agreement. One strength of the model is that it provides a framework for analyzing changes in radiative fluxes for any given set of surface temperature, ocean heat content, OLR, and TOA incoming solar data sets, and identifies which variables are contributing to each flux change. The weakness of such an impartial model as this is that it offers no root-cause explanation or mechanisms for changes in the determining variables S , B , ϵ , or a . These must be determined independently. Thus, for Earth, the model identifies a weakening of the greenhouse effect, and a decreasing planetary albedo, without giving a cause. Decreasing atmospheric water vapor was tentatively identified as a possible cause, but supporting evidence must be sought elsewhere, as it is not available in the model. Another limitation is that the adiabatic model provides no insight into the internal structure and dynamics of the atmosphere: however, the boundary fluxes at the base and top of atmospheres are firmly defined.

The results of the application of the adiabatic model do not negate that the increase in non-condensing atmospheric greenhouse gases in Earth's atmosphere drives an increase in the surface temperature. It is quite clear that increasing ϵ will drive an increase in the surface flux; however, the influence of atmospheric water vapor variability appears to be a determining factor in the behavior of bulk atmospheric emissivity.

To further illustrate the utility of the adiabatic model, Table 3 below compares the output of the adiabatic model with the mean of the 22 CMIP5 / IPCC AR5 models used by Wild et al. (2013) [3] (p. 3114). The values differ slightly from the Wild et al. (2015) energy budget of Figure 5. First, the adiabatic model determines the variables S , B , μ , ϵ , and a directly from the mean of the CMIP5 models, and then applies these variables to the "Value" column of Table 1, which are derived from the radiative model of Figure 4. Values for L and Q are also taken directly from the CMIP5 models. Surface components are well matched by the adiabatic model, and are well within the error margins, with differences less than 0.5 W/m^2 .

One feature of the equilibrium model is the independence of the outgoing longwave radiation and the bulk atmospheric emissivity. In Equation (4), ϵ and T_0 are not independent variables; the outgoing longwave radiation in the equilibrium model shown in Figure 3 depends only on the independent variables solar insolation S and bond albedo a . If I treat solar insolation S as a constant, which is a reasonable approximation, then there are only two ways to significantly change average planetary surface temperature: by changes in P through change in albedo, and by changes in the bulk atmospheric emissivity through altering greenhouse gas abundances. Consider an increase in bulk atmospheric emissivity at a constant value for P . The model predicts that during the resulting non-equilibrium state, OLR will initially decrease due to B . From an energy perspective, this is because the upward surface flux is the only available energy source for increasing the surface temperature, which is rerouted to the surface as part of the increased downwelling component $\epsilon(P - B)/(1 - \epsilon)$ of longwave radiation in Figure 4, and the energy must be deducted from the OLR. When $B = 0$ and equilibrium is regained, the OLR returns to its initial value. Surface flux will increase during the non-equilibrium stage. Conversely, a reduction of ϵ with constant P will result in a transient increase in OLR to $(P - B)$, $B < 0$, during the non-equilibrium state, and OLR will return to its initial value when $B = 0$ and equilibrium is regained; meanwhile, surface flux will decrease during the non-equilibrium stage. Neither of these situations describes the evolution of the Earth's radiative fluxes over the period from 1979–2015, which shows increasing OLR in excess of B and increasing surface flux in a non-equilibrium state.

Table 3. Comparison of 22 Coupled Model Intercomparison Project Phase 5 (CMIP5)/ International Satellite Cloud Climatology Project (IPCC) AR5 models with the adiabatic radiative model. Modified after Wild et al. (2013).

Variables	CMIP5	Adiabatic Model	Difference
$S \text{ W/m}^2$		1364.8	
μ		0.310	
ϵ		0.401	
a		0.300	
$B \text{ W/m}^2$		1.00	
$P = (1 - a)S/4 \text{ W/m}^2$		238.9	
TOA components	Mean W/m^2	W/m^2	W/m^2
Solar down	341.2	341.2	0
Solar up	102.3	102.3	0
Solar net	238.9	238.9	0
Thermal up	237.9	237.9	0
Atmospheric components			
Solar net	74	74	0
Thermal net	179.2	178.8	-0.4
Surface components			
Solar down	189.4	not used	
Solar up	24.8	not used	
Solar net	164.8	164.9	0.1
Thermal down	338.2	337.8	-0.4
Thermal up	396.9	396.9	0
Thermal net	-58.7	-59.1	-0.4
Net radiation	106.2	105.8	-0.4
Latent heat	85.4	$L = 85.4$	
Sensible heat	19.4	$Q = 19.4$	

Increasing P at constant ϵ will drive increases in both surface flux and OLR during the non-equilibrium state, and the energy source is additional solar insolation entering the system due to a reduction in albedo. Increasing P at constant ϵ will also drive an increase in downwelling longwave radiation, because the components $\mu P + \epsilon(P - B)/(1 - \epsilon)$, as shown in Figure 4, will also increase. This situation better describes the behavior of the Earth’s radiative fluxes over the period from 1979–2015. Changes in downwelling longwave radiation cannot be attributed solely to an increase in ϵ without reference to changes in components P and B .

Further clarification of downwelling longwave radiation is required. Some authors (e.g., Trenberth et al. 2009 [23]) refer to this quantity as back radiation. Recall from Figure 4 that downwelling longwave radiation comprises $\mu P + \epsilon(P - B)/(1 - \epsilon) + L + Q$. For the purposes of this study, back radiation strictly refers to surface-emitted longwave radiation, which is absorbed by the atmosphere and re-emitted to the surface, and is the quantity $\epsilon(P - B)/(1 - \epsilon)$. It is the only component of the downwelling longwave radiation with partial dependence on ϵ .

Figure 10 shows the 1979–2015 time-series behavior of the components of downwelling longwave radiation generated by the model. Here, neither P nor ϵ are constant. The component $\epsilon(P - B)/(1 - \epsilon) = \epsilon\sigma T_0^4$, our back radiation, in Figure 10 has seen a downward trend over the period, which is driven by a decreasing greenhouse factor. The component μP , which is atmosphere-absorbed incoming solar re-radiated as longwave toward the surface, has increased due to increased P , assuming constant atmospheric short wave emissivity $\mu = 1/3$. The rate of non-radiative surface-to-atmosphere heat transfer $L + Q$ is assumed to be a constant value of 103 W/m^2 over the same period. The sum of these components, as shown in the top curve in Figure 10, shows an increase in total downwelling longwave radiation over the period, which is driven by μP . Therefore, it is quite possible for total downwelling longwave radiation to increase, even when the greenhouse effect expressed through back radiation decreases. The graph demonstrates the principle,

although the uncertainties associated with OLR used in the derivation of atmospheric absorbed solar and back radiation are significant.

Therefore, change in the time-series magnitude of total downwelling longwave radiation by itself is not diagnostic of any particular change in the greenhouse effect. The greenhouse factor, $1/(1 - \epsilon)$, which is independent of P , B , L , and Q , and is a function only of the bulk atmospheric emissivity with respect to surface emission, provides a more direct and unambiguous measure of the strength of the greenhouse effect.

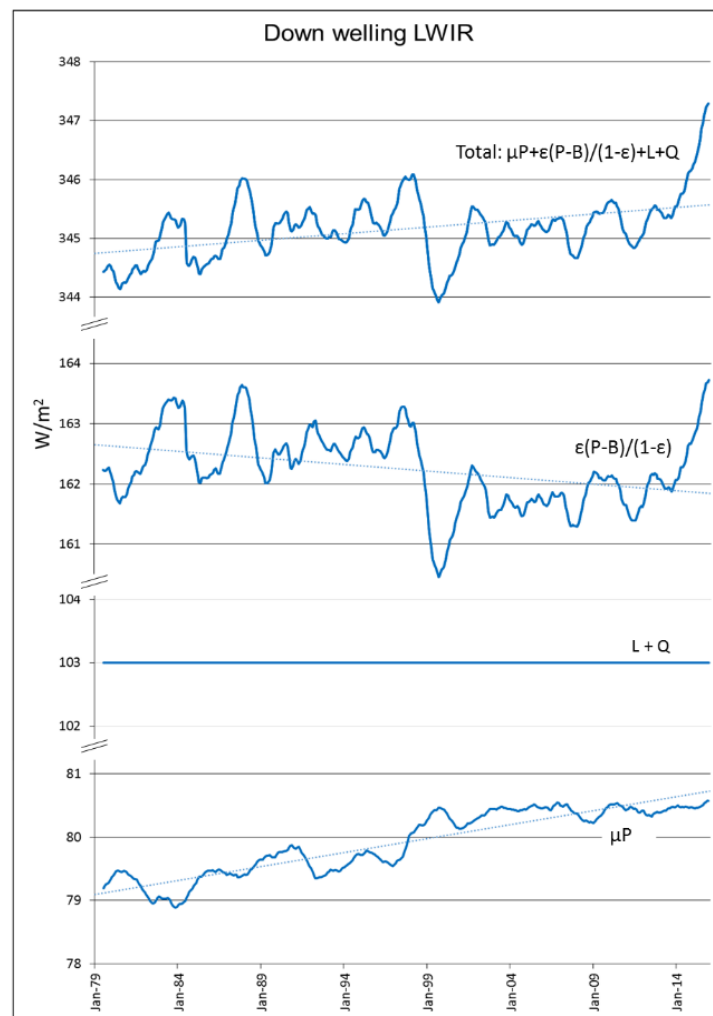


Figure 10. Components of downwelling longwave radiation, 1979–2015. μP is atmosphere-absorbed solar re-emitted as longwave down; $\epsilon(P - B)/(1 - \epsilon)$ is back radiation; $L + Q$ is rate of transfer of latent and specific heat into the atmosphere. Center-averaged 12-monthly values. Blue dotted lines are trend lines. Uncertainty ranges not shown. All of the units are in W/m^2 .

Another feature of the model is that outgoing radiation is sourced entirely from the surface emission; the only route for absorbed solar energy to leave the system is by re-emission from the surface. This is a direct consequence of the non-radiating top of atmosphere, which prevents the atmosphere from radiating directly to space.

Acknowledgments: The study received no funding.

Conflicts of Interest: The author declares no conflict of interest.

References

- Rossow, W.B.; Zhang, Y.-C. Calculation of surface and top of atmosphere radiative fluxes from physical quantities based on ISCCP data sets. 2. Validation and first results. *J. Geophys. Res. Atmos.* **1995**, *100*, 1167–1197. [[CrossRef](#)]
- Kiehl, J.T.; Trenberth, K.E. Earth's annual global mean energy budget. *Bull. Am. Meteorol. Soc.* **1997**, *78*, 197–208. [[CrossRef](#)]
- Wild, M.; Folini, D.; Schär, C.; Loeb, N.; Ellsworth, G.D.; König-Langlo, G. The global energy balance from a surface perspective. *Clim. Dyn.* **2013**, *40*, 3107–3134. [[CrossRef](#)]
- Wild, M.; Folini, D.; Hakuba, M.Z.; Schär, C.; Seneviratne, S.I.; Kato, S.; Rutan, D.; Ammann, C.; Wood, E.F.; König-Langlo, G. The energy balance over land and oceans: An assessment based on direct observations and CMIP5 climate models. *Clim. Dyn.* **2015**, *44*, 3393–3429. [[CrossRef](#)]
- Wild, M.; Ohmura, A.; Schar, C.; Muller, G.; Folini, D.; Schwarz, M.; Hakuba, M.Z.; Sanchez-Lorenzo, A. The Global Energy Balance Archive (GEBA) version 2017: A database for worldwide measured surface energy fluxes. *Earth Syst. Sci. Data* **2017**, *9*, 601–613. [[CrossRef](#)]
- Lee, H.T.; NOAA CDR Program. *NOAA Climate Data Record (CDR) of Daily Outgoing Longwave Radiation (OLR)*; Version 1.2; NOAA National Climatic Data Center: Asheville, NC, USA, 2011. [[CrossRef](#)]
- Fröhlich, C. Observations of irradiance variations. *Space Sci. Rev.* **2000**, *94*, 15–24. [[CrossRef](#)]
- Huang, B.; Thorne, P.W.; Banzon, V.F.; Boyer, T.; Chepurin, G.; Lawrimore, J.H.; Menne, M.J.; Smith, T.M.; Vose, R.S.; Zhang, H.-M. *NOAA Extended Reconstructed Sea Surface Temperature (ERSST)*; Version 5; NOAA National Centers for Environmental Information: Asheville, NC, USA, 2017.
- Fan, Y.; van den Dool, H. A global monthly land surface air temperature analysis for 1948–present. *J. Geophys. Res.* **2008**, *113*, D01103. [[CrossRef](#)]
- KNMI Climate Explorer. Available online: <https://climexp.knmi.nl/start.cgi?id=someone@somewhere> (accessed on 10 December 2017).
- Rossow, W.B.; Schiffer, R.A. Advances in understanding clouds from ISCCP. *Bull. Am. Meteorol. Soc.* **1999**, *80*, 2261–2288. [[CrossRef](#)]
- NVAP Science Team. *NVAP-M Data*; Atmospheric Science Data Center (ASDC): Hampton, VA, USA, 2013. Available online: https://eosweb.larc.nasa.gov/project/nvap/climate_total-precipitable-water_table (accessed on 10 December 2017).
- Vonder Haar, T.H.; Bytheway, J.L.; Forsythe, J.M. Weather and climate analyses using improved global water vapor observations. *Geophys. Res. Lett.* **2012**, *39*, L16802. [[CrossRef](#)]
- Cheng, L.; Trenberth, K.; Fasullo, T.; Boyer, T.; Abraham, J.; Zhu, J. Improved estimates of ocean heat content from 1960 to 2015. *Sci. Adv.* **2017**, *3*, e1601545. [[CrossRef](#)] [[PubMed](#)]
- Yelle, R.V.; Strobel, D.F.; Lellouch, E.; Gautier, D. Engineering Models for Titan's Atmosphere. In *Huygens: Science, Payload and Mission, Proceedings of an ESA Conference, Noordwijk, The Netherlands, 22–25 April 1997*; Wilson, A., Ed.; ESA: Paris, France, 1997; pp. 243–256.
- Wielicki, B.A.; Barkstrom, B.R.; Harrison, E.F.; Lee, R.B.; Smith, G.L.; Cooper, J.E. Clouds and the earth's radiant energy system (CERES): An earth observing system experiment. *Bull. Am. Meteorol. Soc.* **1996**, *77*, 853–868. [[CrossRef](#)]
- Gerlich, G.; Tscheuschner, R.D. On the Barometric Formulas and Their Derivation from Hydrodynamics and Thermodynamics. 2010. Available online: <http://arxiv.org/pdf/1003.1508> (accessed on 10 December 2017).
- Hansen, J.; Nazarenko, L.; Ruedy, R.; Sato, M.; Willis, J.; Del Genio, A.; Koch, D.; Lacis, A.; Lo, K.; Menon, S.; et al. Earth's energy imbalance: Confirmation and implications. *Science* **2005**, *308*. [[CrossRef](#)] [[PubMed](#)]
- NASA Planetary Fact Sheets. Available online: <https://nssdc.gsfc.nasa.gov/planetary/planetfact.html> (accessed on 10 December 2017).
- Lee, H.T.; Gruber, A. Development of the HIRS Outgoing Longwave Radiation Climate Dataset. *Am. Meteorol. Soc.* **2007**. [[CrossRef](#)]
- Morice, C.P.; Kennedy, J.J.; Rayner, N.A.; Jones, P.D. Quantifying uncertainties in global and regional temperature change using an ensemble of observational estimates: The HadCRUT4 dataset. *J. Geophys. Res.* **2012**, *117*, D08101. [[CrossRef](#)]

22. Palle, E.; Goode, P.R.; Montañés-Rodríguez, P.; Shumko, A.; Gonzalez-Merino, B.; Lombilla, C.M.; Jimenez-Ibarra, F.; Shumko, S.; Sanroma, E.; Hulist, A.; et al. Earth's albedo variations 1998–2014 as measured from ground-based earthshine observations. *Geophys. Res. Lett.* **2016**, *43*, 4531–4538. [[CrossRef](#)]
23. Trenberth, K.E.; Fasullo, J.T.; Kiehl, J. Earth's Global Energy Budget. *Bull. Am. Meteor. Soc.* **2009**, *90*, 311–324. [[CrossRef](#)]



© 2018 by the author. Licensee MDPI, Basel, Switzerland. This article is an open access article distributed under the terms and conditions of the Creative Commons Attribution (CC BY) license (<http://creativecommons.org/licenses/by/4.0/>).